TIG 熔敷 Ti-Si-C 系统在 Ti-5Al-2.5Sn 表面形成陶瓷涂层的化学反应分析

闫文青[1,2]， 桂赤斌[2]， 戴 乐[3]

(1. 武汉科技大学 钢铁冶金及资源利用省部共建教育部重点实验室，武汉 4300813;
2. 华南理工大学 机械与汽车工程学院，广州 510641;
3. 河南柴油机集团有限责任公司 407 厂，洛阳 471039)

摘 要: 采用 TIG 热源在钛合金表面堆焊 Ti-SiC 和 Ti-SiC-C 两种体系的粉末，形成表面陶瓷涂层. 利用 SEM 和 XRD 等分析手段对两种配方陶瓷涂层的微观组织和物相进行了分析，用热力学方法计算了两种系统中各种可能发生的化学反应的 Gibbs 自由能变化. 结果表明，Ti-SiC 系统熔敷层的微观组织主要由树枝状的 TiC、针棒状和菊花状的 Ti_5Si_3 相组成，其反应机理为: $8Ti + 3SiC \rightarrow 3TiC + Ti_5Si_3$. Ti-SiC-C 系统熔敷层的微观组织除了树枝状的 TiC 相之外，还有 $TiSi_2$ 和 Ti_3SiC_2，其反应机理为: $6Ti + 3SiC + C \rightarrow Ti_3SiC_2 + TiSi_2 + 2TiC$. 通过对两种系统的微观组织及化学反应分析可得出，在 Ti-SiC 系统中适当的添加石墨，可生成具有自润滑性能的 Ti_3SiC_2 相，避免 Ti_5Si_3 脆性相的生成.

关键词: 钨极氩弧焊熔敷; 陶瓷涂层; 反应机理; 热力学分析
中图分类号: TB 333 **文献标识码**: A **文章编号**: 0253 - 360X(2014) 10 - 0077 - 04

0 序 言

钛合金硬度低，摩擦系数大，在有耐磨损要求的场合，需要对其表面进行改性，使之具有一定的耐磨性. 目前提高钛合金表面硬度的方法一般是在钛合金表面形成一层硬涂层，其方法有激光熔敷、电火花沉积、电弧熔敷和钎焊等工艺[1-4]. 将陶瓷与金属复合，充分发挥金属和陶瓷的各自优点，无疑是冲蚀磨损条件下耐磨材料开发和选择的一个方向. 研究表明硬质陶瓷颗粒如 TiC，TiN，SiC 颗粒等典型修复层的引入可以大大提高钛合金的表面硬度[1-4]，从而提高钛合金表面的耐磨性能. 钛合金焊接常采用钨极氩弧焊(TIG) 方法[5].

文中采用 TIG 熔敷方法，使涂层与基体之间形成冶金结合，在 TA7(Ti-5Al-2.5Sn) 钛合金表面制备了以 TiC 颗粒为主的增强涂层，分析了熔敷过程中出现的化学反应，得出了 Ti-SiC 和 Ti-SiC-C 两种粉末系统在 TIG 电弧热作用下的化学反应机理，并对熔敷层的洛氏硬度进行了测试分析，研究结果对于进一步改善涂层配方具有理论指导意义.

收稿日期: 2013 - 04 - 01
基金项目: 湖北省教育厅资助项目(010403)

1 试验方法

试验用钛板牌号为 TA7，其化学成分见表 1. 试验用熔敷材料为经过充分混合的粉料，用有机粘接剂粘接、滚搓制备的直径约 5 mm 的棒条，经过 150 ℃烘干后用 TIG 焊在 TA7 钛合金表面堆焊，工艺参数为: 焊接电流 350 A，电弧电压 20 U，焊接速度 1.5 mm/s，钨极直径 4 mm，高纯氩气的流量为 0.3 L/s，电弧长度约为 3 mm. 所形成的堆焊焊道见图 1. 试样编号为 S_1 和 S_2. 混合粉由钛粉、SiC 粉及石墨粉按一定比例配制. 配方见表 2. 采用线切割的方法沿垂直焊道横截面的方向进行切割，切取 10 mm × 10 mm × 5 mm 的试样，试样经过砂纸磨平后抛光，用 $HNO_3/HF/2H_2O$ 的腐蚀液进行腐蚀. 用扫描电镜(SEM) 和元素能谱(EDS) 分析进行微观组织分析，用 X 射线衍射分析法(XRD) 进行物相分析，使用型号为 HR-150DT 的洛氏硬度计测试熔敷层的硬度，测试结果为 5 个点的平均值.

表 1 TA7 的化学成分(质量分数，%)

Table 1 Chemical compositions of TA7

Al	Sn	Fe	C	N	H	O	Ti
4.0 ~ 6.0	2.0 ~ 3.0	0.5	≤0.008	≤0.05	≤0.015	≤0.20	余量

(a) 配方为Ti-SiC系统

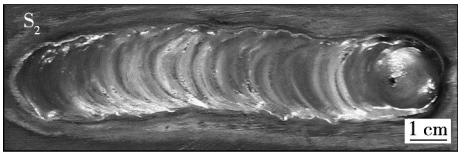

(b) 配方为Ti-SiC-C系统

图 1 熔敷层形貌

Fig. 1 Photos of cladding layers

表 2 试样 S_1 和 S_2 的配方(质量分数,%)

Table 2 Conmponent of sample S_1 and S_2

试样	Ti(200 目)	SiC(60 目)	石墨(200 目)
S_1	80	20	—
S_2	80	10	10

2 试验结果及其分析

图 2 为试样 S_1 和 S_2 焊缝横截面的 SEM 显微组织. 图 3 为试样 S_1 和 S_2 焊缝表面的 XRD 图谱. 根据 XRD 物相检测结果及结合 EDS 分析(表 3),对图 2 中的不同物相进行了分析. 分析结果得出,试样 S_1 中的物相为 SiC,TiC,Ti_5Si_3;而试样 S_2 中除了 SiC 和 TiC 外,还有 $TiSi_2$ 和 Ti_3SiC_2 相,如图 2 中标记所示. 从图 2 可以看出有少量大块的 SiC 颗粒嵌入熔敷层,由 SEM 结合 EDS 分析得出在 SiC 颗粒周围主要分布着树枝状的 TiC 相. 试样 S_1 和 S_2 的主要区别是:S_1 试样中 TiC 周围有位向不同的针状或者菊花状的 Ti_5Si_3 相组成,而在试样 S_2 中 TiC 周围主要分布着 $TiSi_2$ 和 Ti_3SiC_2 相. 电弧熔池的温度一般在 1 770 ℃ 左右,因此从热力学方面计算 1 770 ℃熔敷层中发生化学反应的 Gibbs 自由能的变化情况. 由式(1) ~式(3),计算反应的 Gibbs 自由能的变化见表 4,其中 ΔH_i^Θ 和 S_i^Θ 的数据由热力学手册[6]获得(表 5),由于 Ti_3SiC_2 的高温热力学数据目前还不能从热力学数据手册上查出,因此根据文献[7]中关于 Ti_3SiC_2 相的 Gibbs 生成自由能的计算方法(表 5)来计算.

$$\Delta G_T^\Theta = \Delta H_{298}^\Theta - T\Delta S_{298}^\Theta \quad (1)$$

$$\Delta H_{298}^\Theta = \sum (n_i \Delta H_{i,f,298}^\Theta)_{生成物} - \sum (n_i \Delta H_{i,f,298}^\Theta)_{反应物} \quad (2)$$

$$\Delta S_{298}^\Theta = \sum (n_i S_{i,298}^\Theta)_{生成物} - \sum (n_i S_{i,298}^\Theta)_{反应物} \quad (3)$$

式中:ΔG_T^Θ 为标准吉布斯自由能;ΔH_{298}^Θ 为标准反应热效应;ΔS_{298}^Θ 为标准反应熵差;n_i 为参与反应各物质中 i 物质的量;$\Delta H^\Theta_{i,f,298}$ 为参与反应各物质 i 在常温下的标准摩尔生成热;$S^\Theta_{i,298}$ 为参与反应各物质 i 在常温下的标准摩尔熵.

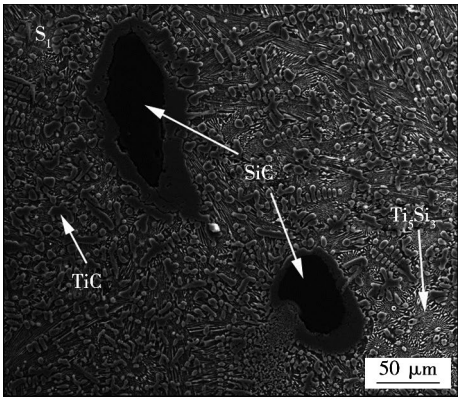

(a) 配方为Ti-SiC系统

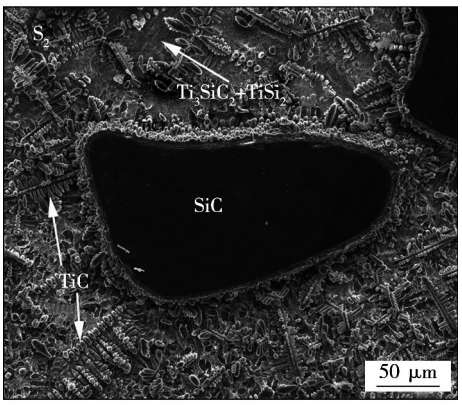

(b) 配方为Ti-SiC-C系统

图 2 试样 S_1 和 S_2 的熔敷层横截面的 SEM 形貌

Fig. 2 SEM graphs of cladding layer for cross

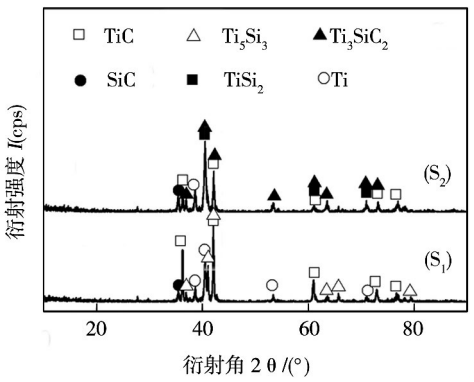

图 3 试样 S_1 和 S_2 的焊缝表面的 XRD 曲线

Fig. 3 XRD patterns of sample S_1 and S_2

Ti-Si-C 系统在 TIG 电弧热源的作用下熔池中

表 3　S_1 和 S_2 熔敷层中各相的 EDS 数据

Table 3　EDS data of phases of S_1 and S_2 in cladding layers

元素含量(原子分数,%)			物相
Ti	Si	C	
48.45	—	51.55	TiC
—	47.42	52.58	SiC
45.72	28.70	25.58	Ti_5Si_3
42.38	32.32	25.30	$Ti_3SiC_2 + TiSi_2$

表 4　1 770 ℃时反应的 Gibbs 自由能的变化

Table 4　Change of Gibbs energy of reactions at 1 770 ℃

	化学反应	1 770 ℃吉布斯自由的变化 ΔG/(kJ·mol^{-1})
(1)	$SiC \rightarrow Si + C$	−41.4
(2)	$Ti + C \rightarrow TiC$	−76.4
(3)	$Ti + 2Si \rightarrow TiSi_2$	159.0
(4)	$3Si + 5Ti \rightarrow Ti_5Si_3$	111.0
(5)	$8Ti + 3SiC \rightarrow 3TiC + Ti_5Si_3$	−680.0
(6)	$3Ti + 2SiC \rightarrow TiSi_2 + 2TiC$	−370.0
(7)	$Ti + SiC \rightarrow TiC + Si$	−118.0
(8)	$10Ti + 4SiC \rightarrow Ti_5Si_3 + 2TiC + Ti_3SiC_2$	−110.0
(9)	$6Ti + 3SiC + C \rightarrow Ti_3SiC_2 + TiSi_2 + 2TiC$	−1 250.0
(10)	$5Ti + TiSi_2 + 4C \rightarrow 2Ti_3SiC_2$	38.0

表 5　Ti-Si-C 三元系统 1 770 ℃时相的热力学数据

Table 5　Thermodynamics data of phases in Ti-Si-C system at 1 770 ℃

相	生成热 $\Delta H_i^{\ominus}$/(J)	摩尔熵 $S_i^{\ominus}$/(J)	Gibbs 自由能表达式
C	0	5.732	
Si	50 208 (>1 685 K)	91.551 (>1 685 K)	
Ti	4 142 (1 155~1 933 K)	72.983 (1 155~1 933 K)	
SiC	−73 220	16.610	
TiC	−184 096	24.225	
$TiSi_2$	−134 306	61.086	
Ti_5Si_3	−579 066	217.986	
Ti_3SiC_2	—	—	$G_m^{Ti_3SiC_2} = 1\,547\,145 + 240\,845T$ [7]

可能发生的化学反应见表 4. 从表 4 中的数据可以看出,SiC 颗粒一部分在熔池温度下发生分解,生成 Si 和 C 原子. Si 原子一部分与熔池中的物质发生化学反应,另外一部分在电弧高温下发生蒸发. 在高温 1 770 ℃左右,Ti 与 Si 和 C 原子分别发生反应,钛与碳反应生成 TiC,反应的 Gibbs 自由能的变化为负值,而钛与硅反应生成 $TiSi_2$ 和 Ti_5Si_3,反应的 Gibbs 自由能的变化为正值,因此钛与硅在熔池温度下以 Ti-Si 液相共晶的状态存在,这也与 Ti-Si 二元相图[7]一致. 说明在熔池高温下,优先形成 TiC 相. 以上分析也解释了两种试样熔敷后所形成的涂层是以 TiC 相为主. 另外一部分 SiC 与 Ti 反应,在试样 S_1 中没有石墨参与的情况下,SiC 与 Ti 反应可能发生 4 种化学反应(见表 4 中的反应(5) ~反应(8)),但从这些化学反应的 Gibbs 自由能的变化可以看出,$8Ti + 3SiC \rightarrow 3TiC + Ti_5Si_3$ 反应所需要的能量最少,生成的产物为 TiC 和 Ti_5Si_3,与 SEM 及 XRD 检测结果相一致. 而在试样 S_2 中有石墨参与的情况下,SiC 与 Ti 反应可能发生只有 $6Ti + 3SiC + C \rightarrow Ti_3SiC_2 + TiSi_2 + 2TiC$,并且反应需要的 Gibbs 自由能的变化为 −1 250 kJ/mol,反应有利于向右进行. 这就是试样 S_2 的涂层中 Ti_3SiC_2、$TiSi_2$ 和 TiC 的生成机理,也说明在钛和 SiC 粉末中加入石墨有利于 Ti_3SiC_2 相的生成,避免了 Ti_5Si_3 脆性相的形成,可以减少涂层开裂的倾向.

Ti_3SiC_2 是目前研究很热的一种新材料,因为它同时具有陶瓷与金属的一些特点,并且像石墨一样具有自润滑性能,有研究表明材料中加入适量的 Ti_3SiC_2 能够提高耐磨性[8,9]. 同时在两种试样中均发现了比较大的 SiC 颗粒,认为是在电弧堆焊时由于快速加热和快速冷却导致 SiC 颗粒没有完全参与反应而残留下来. 文中采用 60 目的 SiC 颗粒,颗粒比较粗大,或许采用细颗粒的 SiC 颗粒作为原材料会提高它参与化学反应的程度,有待于后续试验进行证实.

洛氏硬度测试表明,试样 S_1 的平均硬度为 59.4 HRC,S_2 的平均硬度为 41.8 HRC. 测试过程中,试样 S_1 的表面压痕周围存在大块涂层脱落现象,而试样 S_2 的表面压痕周围没有大块涂层脱落现象,但是有少量的裂纹出现. 说明试样 S_1 与试样 S_2 相比脆性较大,其主要原因是脆而硬的 Ti_5Si_3 相造成的,而试样 S_2 中低硬度、层状结构相 Ti_3SiC_2 对裂纹的扩展起了阻止作用,提高了涂层的韧性.

3　结　论

(1) 试样 S_1(Ti-SiC 系统)熔敷后形成的涂层中主要为 TiC 和 Ti_5Si_3 两相,而试样 S_2(Ti-SiC-C 系统)熔敷后形成的涂层中主要为 TiC,$TiSi_2$ 和 Ti_3SiC_2 三相组成,同时两种系统中均有少量未完全参与化学反应的 SiC 残留.

(2) 两种粉末系统在 TIG 电弧热源作用下的反应机理分别是:$8Ti + 3SiC \rightarrow 3TiC + Ti_5Si_3$ 和 $6Ti + 3SiC + C \rightarrow Ti_3SiC_2 + TiSi_2 + 2TiC$. 石墨的加入导致

了 Ti_3SiC_2 相的生成，避免了金属间化合物 Ti_5Si_3 脆性相的形成.

(3) 硬度测试表明试样 S_2 的熔敷涂层的洛氏硬度较低，为 41.8 HRC，并且硬度压痕周围不存在块状脱落现象，只有少量的裂纹出现.

参考文献:

[1] Zhang S, Wu W T, Wang M C, *et al*. Laser induced TiC particle reinforced composite layer on Ti6Al4V and their microstructural characteristics [J]. Transactions of Nonferrous Metals Society of China, 2000, 10(1): 6 - 9.

[2] 郝建军，彭海滨，黄继华，等. 钛合金表面电火花沉积 TiN/Ti 复合涂层 [J]. 焊接学报，2009，30(11)：69 - 72.
Hao Jianjun, Peng Haibin, Huang Jihua, *et al*. TiN/Ti composite coating deposited on titanium alloy substrate by reactive electrie-spark [J]. Transactions of the China Welding Institution, 2009, 30(11): 69 - 72.

[3] 王振廷，陈丽丽，张显友. 钛合金表面氩弧熔敷 TIC 增强复合涂层组织与性能分析 [J]. 焊接学报，2008，29(9)：43 - 45.
Wang Zhenting, Chen Lili, Zhang Xianyou. Microstructure and properties of TiC reinforced composite coating fabricated on Ti alloy by GRAW [J]. Transactions of the China Welding Institution, 2008, 29(9): 43 - 45.

[4] 崔 冰，黄继华，熊进辉，等. TiC 增强 C_f/SiC 复合材料与钛合金钎焊接头工艺分析 [J]. 焊接学报，2012，33(3)：85 - 88.
Cui Bing, Huang Jihua, Xiong Jinhui, *et al*. Analysis of brazed joints between carbon fiber reinforced SiC composite and titanium alloy with TiC [J]. Transactions of the China Welding Institution, 2012, 33(3): 85 - 88.

[5] Wang M, Dong Z B, Yu L, *et al*. Numerical simulation of temperature fields for T-joint during TIG welding of titanium alloy [J]. China Welding, 2008, 17(3): 6 - 9.

[6] 叶大伦，胡建华. 实用无机物热力学数据手册 [M]. 2 版，北京：机械工业出版社，2009.

[7] Du Y, Schuster J C, Seifert H J, *et al*. Experimental investigation and thermodynamic calculation of the titanium-silicon-carbon system [J]. Journal of America Ceramics Society, 2000, 83(1): 197 - 203.

[8] Fan X, Yin X W, He S S, *et al*. Friction and wear behaviors of C/C-SiC composites containing Ti_3SiC_2 [J], Wear, 2012, 274/275(1): 188 - 195.

[9] Shi X L, Wang M, Zhai W Z, *et al*. Influence of Ti_3SiC_2 content on tribological properties of NiAl matrix self-lubricating composites [J]. Materials and Design, 2013, 45(3): 179 - 189.

作者简介: 闫文青，女，1977 年出生，博士，副教授. 主要从事有色金属和复合材料连接方面的科研和教学工作. 发表论文 9 篇. Email: yanwenqing77@163.com

[上接第 76 页]

Wang Honghong, Zhang Hanqian, Sun Xian. Analysis of microstructure characteristic of 9% Cr ~ 1% Mo heat resistant steel weld metal [J]. Transactions of the China Welding Institution, 2008, 29(9): 91 - 95.

[6] 李轶非，王 梁，吴健栋，等. NiCrMoV 耐热钢贝氏体焊缝韧性薄弱区的确定 [J]. 机械工程学报，2013，49(4)：83 - 88.
Li Yifei, Wang Liang, Wu Jiandong, *et al*. Determination of toughness weak points of bainite weld metal of NiCrMoV refractory steel [J]. Journal of Mechanical Engimeering, 2013, 49(4): 83 - 88.

[7] 徐向星，苏 毅，周 伟，等. M-A 组元与粒状贝氏体焊缝的解理断裂 [J]. 金属学报，1988，24(5)：361 - 365.
Xu Xiangxing, Su Yi, Zhou Wei, *et al*. Relationship between M-A constituent and cleavage fracture behavior of acicular bainitic weld metal [J]. Acta Metallurgica Sinica, 1988, 24(5): 361 - 365.

[8] Zhang B W, Wei J S, Zhang T H. A study of local brittle zone (LBZ) of 10Ni5CrMoV steel after double thermal cycles [J]. China Welding, 2005, 14(2): 149 - 152.

[9] 张英乔，张汉谦，刘伟明. M-A 组元对石油储罐用钢粗晶热影响区韧性的影响 [J]. 焊接学报，2009，30(1)：109 - 112.
Zhang Yingqiao, Zhang Hanqian, Liu Weiming. Effects of M-A constituent on toughness of coarse grain heat affected zone in HSLA steels for oil tanks [J]. Transactions of the China Welding Institution, 2009, 30(1): 109 - 112.

[10] 王 学，常建伟，黄关政，等. WB36 钢临界再热粗晶区组织性能 [J]. 焊接学报，2008，29(10)：29 - 32.
Wang Xue, Chang Jianwei, Huang Guanzhen, *et al*. Study on microstructure and properties of IRCGHAZ in WB36 [J]. Transactions of the China Welding Institution, 2008, 29(10): 29 - 32.

作者简介: 李轶非，男，1989 年出生，博士研究生. 主要研究方向为焊接结构和焊接冶金的理论与工程. 发表论文 4 篇. Email: dmeliyifei@gmail.com

通讯作者: 蔡志鹏，男，博士，副研究员. Email: czpdme@mail.tsinghua.edu.cn

toughness is closely related to the distribution, pattern and dimension. M-A constituents in the refined zone of welded layers decompose at second peak temperature of 680 ℃, large particle M-A constituents at prior austenite grain boundaries and bulk grain M-A constituents in prior austenite grains are found in the incomplete phase change zone of welded layers at second peak temperature of 820 ℃, and M-A constituents distribute uniformity at 1 050 ℃ with the disappear of prior austenite grain boundaries.

Key words: weld toughness; M-A constituent; refractory steel; incomplete phase transition zone

Chemical reaction of ceramic coatings of Ti-Si-C system on Ti-5Al-2.5Sn substrate prepared by tungsten inert-gas arc cladding YAN Wenqing[1,2], GUI Chibin[2], DAI Le[3] (1. Key Laboratory for Ferrous Metallurgy and Resources Utilization of Ministry of Education, Wuhan University of Science and Technology, Wuhan 430081, China; 2. School of Mechanical and Automotive Engineering, South China University of Technology, Guangzhou 510641, China; 3. Military Representative Office of Navy, Henan Diesel Engine Group Limited Company 407 Factory, Luoyang 471039, China). pp 77 - 80

Abstract: The surface ceramic coatings were prepared on Ti-5Al-2.5Sn substrate by tungsten inert-gas arc depositon process. The microstructures and phases were analyzed using the method of SEM and XRD for the cladding coatings of Ti-SiC and Ti-SiC-C systems. Moreover, the changes of Gibbs energy for possible reactions in systems were calculated using thermodynamic analysis. The results shows that the main microstructure are composed with dendritic TiC and needle-shaped or chrysanthemum Ti_5Si_3 in the cladding coating of Ti-SiC system, the reaction mechanism is $8Ti + 3SiC \rightarrow 3TiC + Ti_5Si_3$. However, in Ti-SiC-C system, there are $TiSi_2$ and Ti_3SiC_2 hybrid microstructure observed besides TiC. $6Ti + 3SiC + C \rightarrow Ti_3SiC_2 + TiSi_2 + 2TiC$ is the main reaction mechanism. In addition, the addition of graphite in Ti-SiC system favors to the generation of self-lubricating Ti_3SiC_2 phases, while the brittle Ti_5Si_3 phases are avoided.

Key words: tungsten inert-gas arc cladding; ceramic coating; reaction mechanism; thermodynamic analysis

Research on scanning path based on metal powder electron beam rapid prototyping CHEN Yunxia[1,2], WANG Xiaojing[3], CHEN Shanben[2], YAO Shun[2] (1. School of Mechanical and Electrical Engineering, Hohai University, Changzhou 213022, China; 2. School of Electronic Information and Electrical Engineering, Shanghai Jiaotong University, Shanghai 200240, China; 3. School of Materials Science and Engineerin, Jiangsu University of Science and Technology, Zhenjiang 212003, China). pp 81 - 84

Abstract: Aimed at the influence of temperature distribution on forming parts caused by scanning paths of filling line of electron beam rapid prototyping technology, finite element model of simultaneous scanning and orderly scanning were established and corresponding experiments were done. The simulation results show that comparing with simultaneous scanning, the forming part quality formed by orderly scanning is better and it can be improved with the offsetting distance shorted. Although with a smaller electron beam current in orderly scanning forming process, the metal powder can also achieved a higher melting temperature and high temperature region, and the forming area is consistent with its scanning area. The equal energy density of each point on the scanning area is help to get relatively smooth forming surface and to easy spread next powder.

Key words: electron beam rapid prototyping; scanning path; energy density; numerical simulation

Microstructure of single track fiber laser cladding with wire feeding by side LI Kaibin, LI Dong, LIU Dongyu, YU Zhishui (School of Material Engineering, Shanghai University of Engineering Science, Shanghai 201620, China). pp 85 - 88

Abstract: Laser cladding was performed on the surface of stainless steel with wire feeding by side. To obtain an optimal combination of process parameters, orthogonal test was used to determine the influences of laser power (P), scanning velocity (v_s) and wire feeding speed (v_w) on the cross-section geometry, aspect ratio and dilution rate of cladding track. The results show that the stable and smooth cladding track can be obtained when the combination of process parameters are $P = 2\ 000$ W, $v_s = 4$ mm/s, and $v_w = 20$ mm/s. Grain morphology of the cladding track from the binding to the surface are planar crystal, cellular crystal, columnar dendrites, equiaxed dendrite, steering dendrites. The microstructure of laser cladding track is composed of γ austenite and residual δ ferrite, and the δ ferrite distributed in the austenite grain boundaries or between dendrites with the vermicular, skeletal and lathy morphologies. The average microhardness of the cladding track is about 195 MPa near to the one of substrate (207 MPa), which is evenly distributed, but the microhardness of heat affected zone (178 MPa) is lower than the one of substrate.

Key words: laser cladding; wire feeding by side; microstructure; microhardness

Numerical simulation and test verification of welding temperature field of 12Cr1MoV heat-resistant steel pipe CHI Luxin, SUN Zhaofan, WU Guangfeng (College of Materials Science and Engineering, Chongqing University of Technology, Chongqing 400050, China). pp 89 - 92

Abstract: To obtain reasonable welding heat input and accurately predict heat affected zone width of 12Cr1MoV heat-resistant steel pipe for controlling boiler welding quality, the thermal circling curves of typical position on steel pipe was obtained by numerical simulation with ANSYS software based on different welding process parameters. Compared the simulation results and the experimental results, it was found that the values calculated of thermal circling curves were close to the ones measured by infrared thermometer. Moverover, the simulation width of welding heat-affected zone was basically the same as the measured value. Welded joint microstructure is mainly acicular ferrite, and heat affected zone microstructure is mainly proeutectoid ferrite and quasi-eutectoid sorbite, while overheated zone have a small amount of ferrite and granular bainite.

Key words: 12Cr1MoV steel; numerical simulation; temperature field; microstructure

Determination of shape parameters of double ellipsoid heat source model in numerical simulation based on SYSWELD software LI Ruiying[1], ZHAO Ming[2], WU Chunmei[1] (1. Department of Physics and Electricity Information Engineering, Daqing Normal University, Daqing 163712, China; 2. College